Supporting Information

Wittmeier *et al.* 10.1073/pnas.0809377105

SI Text

Model Description. The preBötC and pFRG pacemaker models of Fig. 1 of the main paper are based on Hodgkin–Huxley formalism as described previously (1). Each pacemaker consists of fast sodium Na_F, delayed rectifier potassium K_{Dr}, persistent sodium Na_P, and leak channels. The membrane potential V of one pacemaker is defined as

$$C_M \cdot \frac{d}{dt}V = -I_{NaF} - I_{KDr} - I_{NaP} - I_{Leak} - I_{Syn} - I_{tonic} \quad [1]$$

where $C_M = 21.2$ pF is the membrane capacitance [consistent with whole-cell capacitance measurements from inspiratory neurons in vitro (2)], and t is time (in milliseconds). The conductances of the ionic currents on the right hand side are regulated by voltage-dependent activation and inactivation gating variables. The dynamics of a gating variable x are described according to

$$\frac{d}{dt}x = \frac{x_\infty(V) - x}{\tau_x(V)} \quad [2]$$

$$x_\infty(V) = \frac{1}{1 + \exp\left[(V - \theta_x)/\sigma_x\right]} \quad [3]$$

$$\tau_x(V) = \frac{\bar{\tau}_x}{\cosh\left[(V - \theta_x)/2\sigma_x\right]}, \quad [4]$$

where $x_\infty(V)$ is the steady-state voltage-dependent (in)activation function of x and $\tau_x(V)$ is the voltage-dependent time constant. The ionic currents of each pacemaker are defined as

$$I_{NaF} = \bar{g}_{NaF} m_\infty^3(V)(1 - n)(V - E_{Na}) \quad [5]$$

$$I_{KDr} = \bar{g}_{KDr} n^4 (V - E_K) \quad [6]$$

$$I_{NaP} = \bar{g}_{NaP}\, k_\infty h (V - E_{Na}) \quad [7]$$

$$I_{Leak} = g_L(V - E_L) \quad [8]$$

$$I_{Syn} = g_{Syn}(t)(V - E_{Syn}) \quad [9]$$

$$I_{tonic} = g_{tonic}(V - E_{tonic}). \quad [10]$$

The parameters for the gating variables, maximum conductances and reversal potentials of the currents I_{NaF}, I_{KDr}, I_{NaP}, I_{Leak} for both pacemakers are listed in Table S1. The parameter values were chosen to represent the desired synaptic coupling and relative pacemaker excitabilities (or spontaneous burst frequencies) that were appropriate for the handshake mechanism.

The mutual synaptic coupling of the pFRG and preBötC in the model comprises excitatory (pFRG to preBötC) and inhibitory (preBötC to pFRG) synaptic input. Hence, the reversal potential of the excitatory synapse was set to $E_{Syn} = -10$ mV (3), whereas that of the inhibitory synapses was $E_{Syn} = -94$ mV (3) or $E_{Syn} = -53$ mV (assuming GABAergic or glycinergic inhibition). Because the specific receptor subtypes of pFRG-preBötC synaptic interactions have not been identified, the time-dependent changes in synaptic conductance was modeled by a single exponential with decay time constant of $\tau = 25$ ms to broadly cover both fast and slow excitatory and inhibitory receptor currents as in ref. 3. Accordingly, the time-dependent conductance $g_{Syn}(t)$ of a synapse is defined as

$$g_{Syn}(t) = \left[g_{Syn}(t_0) + g_{E/I}\right] \exp^{(t_0 - t)/\tau} \quad [11]$$

where t_0 is the time of the most recent event. The synaptic conductance increase associated with 1 synaptic event was set to $g_E = 0.12$ nS for the excitatory and $g_I = 1$ nS for the inhibitory synapses, unless specified otherwise. The threshold for spike detection was 0 mV, the delay for synaptic event transmission from neuron a to b was set to 0 ms.

The tonic input current I_{tonic} was used to model the post-I feedback inhibition of the preBötC pacemaker during the pre-I rebound burst and hence was only included in the preBötC pacemaker. Because the precise neural mechanism of this "inspiratory off-switch" is presently unknown, no attempt was made to model this process in detail except to note that the timing, duration and magnitude of the post-I inhibitory feedback should appropriately gate off the excitatory input from the pFRG without inducing postinhibitory rebound excitation in the preBötC. I_{tonic} was equal to 0 by default and was set to I_{tonic} (nA) = g_{tonic} (nS)·(V + 94 mV) with $g_{tonic} = 0.2$ nS for the duration of the pFRG rebound burst.

For the opioid-induced quantal breathing simulations a stochastic synapse was substituted for the deterministic excitatory preBötC synapse. The conductance of this synapse was based on a Gaussian distribution with mean conductance $\mu_E = g_E = 0.12$ nS and variance $\sigma_E = 0.5 \cdot g_E = 0.06$ nS (default settings). Every time a pFRG spike was detected a new synaptic conductance was picked from the distribution and assigned to g_E. Negative values of g_E are not physiological and hence were set to 0. An example for the distribution of the synaptic conductance with mean $\mu_E = 0.12$ nS and variance $\sigma_E = 0.06$ nS is shown in Fig. S2*B*.

Simulations were performed on the NEURON simulator platform (4). The first 10–20 s of each simulation run were neglected to allow transients to decay. Simulation results were analyzed using custom written software implemented in NEURON, C++, and Matlab, and parameters of interest such as inspiration time (t_I), expiration time (t_E), cycle time (t_C), etc. were extracted. For the distinction between an interspike and interbust interval a predefined threshold time of 200 ms was used.

Simulation of pFRG Stimulation. We showed that stimulation of the pFRG pacemaker evoked a premature preBötC burst when the time between the preceding preBötC cycle and the stimulation was >66% of the preBötC cycle duration. This phenomenon arises from the combined effect of the 2 following intrinsic properties of the pFRG and preBötC pacemaker (Fig. S1):

pFRG. The inactivation gating variable of the burst generating persistent sodium channel h decreases during the burst and increases during the interburst interval. Hence, a stimulus applied later during the interburst interval can evoke a burst with a higher discharge frequency (especially for later spikes in the burst) which results in a stronger excitation of the preBötC pacemaker.

preBötC. Here too, h decreases during the burst and increases during the interburst interval. Hence, a later stimulation results in a higher value of h, which increases the excitability of the preBötC pacemaker.

Simulation of Opioid-Induced Quantal Breathing. Opioid-induced quantal breathing after application of μ-receptor agonists, such

as DAMGO (5) or fentanyl (6), has been proposed to originate from "transmission failure of periodic drive from unaffected pre-I neurons to depressed preBötC networks" (5). The preBötC depression is hypothesized to result from pre- and postsynaptic suppression (7) as modeled in the main paper by: (*i*) preBötC hyperpolarization (≈3.0 mV) and (*ii*) reduced Gaussian-distributed excitatory drive from the pre-I neuron (μ_E = 0.105 nS, σ_E = 0.0525 nS; 87.5% of control). Here, we show that under control conditions (no hyperpolarization, no synaptic suppression) no preBötC cycle is skipped and all preBötC cycle durations are distributed around the baseline cycle time (Fig. S2*A*). Furthermore, by investigating the individual effect of pre- and postsynaptic preBötC suppression, we demonstrate that a distribution of the skipped respiratory cycles as observed experimentally after fentanyl application (6) requires the modeling of both pre- and postsynaptic preBötC suppression (Fig. S2*C* and *D* and Fig. S3).

Presynaptic Suppression. The effect of presynaptic preBötC suppression on the distribution of respiratory cycle durations has been investigated. The mean and variance of the excitatory stochastic preBötC synapse (μ_E and σ_E, respectively) were hereby gradually decreased from 100% to 50% in steps of 5% (Fig. S3*A*). The simulation results show that a decrease in synaptic strength causes a shift in the distribution of the skipped cycle probabilities from a $n = 0$ (55–100%) to a $n = 1$ (50%) dominant distribution. Moreover, for all tested levels of synaptic strength, at most two respiratory cycles were skipped.

Postsynaptic Suppression. Postsynaptic preBötC suppression was investigated by gradual reduction of the leak reversal potential E_L (−61 mV to −63 mV in steps of −0.2 mV). We found that the probability for skipping more than one preBötC cyle ($n > 0$) and the maximum number of skipped cycles gradually increased for higher hyperpolarizations (Fig. S3*B*). For leak reversal potentials lower than −63 mV even more than the experimentally observed three cycles were skipped (not shown) and hence these simulations were not further considered.

These simulation results show that neither pre- nor postsynaptic preBötC suppression alone can account for the distribution of skipped respiratory cycles observed experimentally. Hence, a combination of pre- and postsynaptic effects as used in the main paper is required to replicate the experimental data.

Double Bursts in Phrenic Discharge Recorded During Recovery from Hypoxia. Recordings were made from urethane-anesthetized, vagotomized, paralyzed, and artificially ventilated adult Sprague–Dawley rats. Experimental methods and procedures are as described previously (8, 9). In this animal (Fig. S4), phrenic nerve discharge exhibited a double-burst pattern after a brief period of hypoxia (18–30 s at 8% O_2 balance nitrogen). Double bursts occurred exclusively during recovery from hypoxia when "posthypoxia frequency decline" (10) was observed. A typical double burst was comprised of a normal burst preceded by a smaller premature burst (arrowheads). The 2 bursts were separated by a brief silent period ("gap") lasting 1–1.2 times that of a normal inspiratory duration.

In this animal, unit discharges were also recorded with an extracellular microelectrode that was inserted into the dorsolateral pons "pneumotaxic" region as described previously (8). Three respiratory units are shown in Fig. S4 *A–C*. The EI (expiratory-to-inspiratory) neuron shown in Fig. S4*A* is a phase-spanning unit with tonic background firing. This unit discharged tonically during the entire respiratory cycle, but the firing frequency was markedly increased from late expiratory to inspiratory phase (see enlarged views in *Insets*). Spike-sorting analysis revealed that all of the recorded spikes (both the tonic background and the superimposed EI discharges) were from the same neuron. In normal respiratory cycles, the phrenic bursts started at around the mid-point of this EI discharge (Fig. S4*A* *Inset* 1). In cycles with double bursts (Fig. S4*A* *Inset* 2), the premature phrenic burst (arrowheads) started almost simultaneously with the beginning of the EI discharge. In Fig. S4*B*), LateE (late expiratory unit) is a neuron that exhibited augmenting firing during the late 1/2–1/3 of expiratory phase. In cycles with double bursts, the unit discharge was terminated by the premature burst but resumed during the interburst "gap," only to be terminated again by the second phrenic burst. In Fig. S4*C*), the wE ("whole-phase" expiratory) unit discharged throughout the entire or almost entire expiratory phase and was kept silent during the normal inspiratory phase. Unlike the lateE neuron, wE was kept silent during the entire double-burst period without any resumption of firing during the interburst "gap." The phase relationships of these respiratory units to the phrenic normal and double bursts confirmed that the double burst comprised a premature inspiratory burst, followed by a normal burst.

1. Butera RJ, Rinzel J, Smith JC (1999) Models of respiratory rhythm generation in the pre-Bötzinger complex. I. Bursting pacemaker neurons. *J Neurophysiol* 82:382–397.
2. Smith JC, Ballanyi K, Richter DW (1992) Whole-cell patch-clamp recordings from respiratory neurons in neonatal rat brainstem in vitro. *Neurosci Lett* 134:153–156.
3. Rybak IA, Paton JF, Schwaber JS (1997) Modeling neural mechanisms for genesis of respiratory rhythm and pattern. II. Network models of the central respiratory pattern generator. *J Neurophysiol* 77:2007–2026.
4. Carnevale, T, Hines, M (2006) *The NEURON Book* (Cambridge Univ Press, Cambridge, UK).
5. Mellen NM, Janczewski WA, Bocchiaro CM, Feldman JL (2003) Opioid-induced quantal slowing reveals dual networks for respiratory rhythm generation. *Neuron* 37:821–826.
6. Janczewski WA, Feldman JL (2006) Distinct rhythm generators for inspiration and expiration in the juvenile rat. *J Physiol* 570:407–420.
7. Takeda S, *et al.* (2001) Opioid action on respiratory neuron activity of the isolated respiratory network in newborn rats. *Anesthesiology* 95:740–749.
8. Song G, Yu Y, Poon CS (2006) Cytoarchitecture of pneumotaxic integration of respiratory and nonrespiratory information in the rat. *J Neurosci* 26:300–310.
9. Song, G, Poon, CS (2008) Lateral parabrachial nucleus mediates shortening of expiration during hypoxia. *Respir Physiol Neurobiol*, doi:10.1016/j.resp.2008.10.007 Available online 17 October, 2008.
10. Coles, SK, Dick, TE (1996) Neurones in the ventrolateral pons are required for post-hypoxic frequency decline in rats. *J Physiol* 497(Pt 1):79–94.

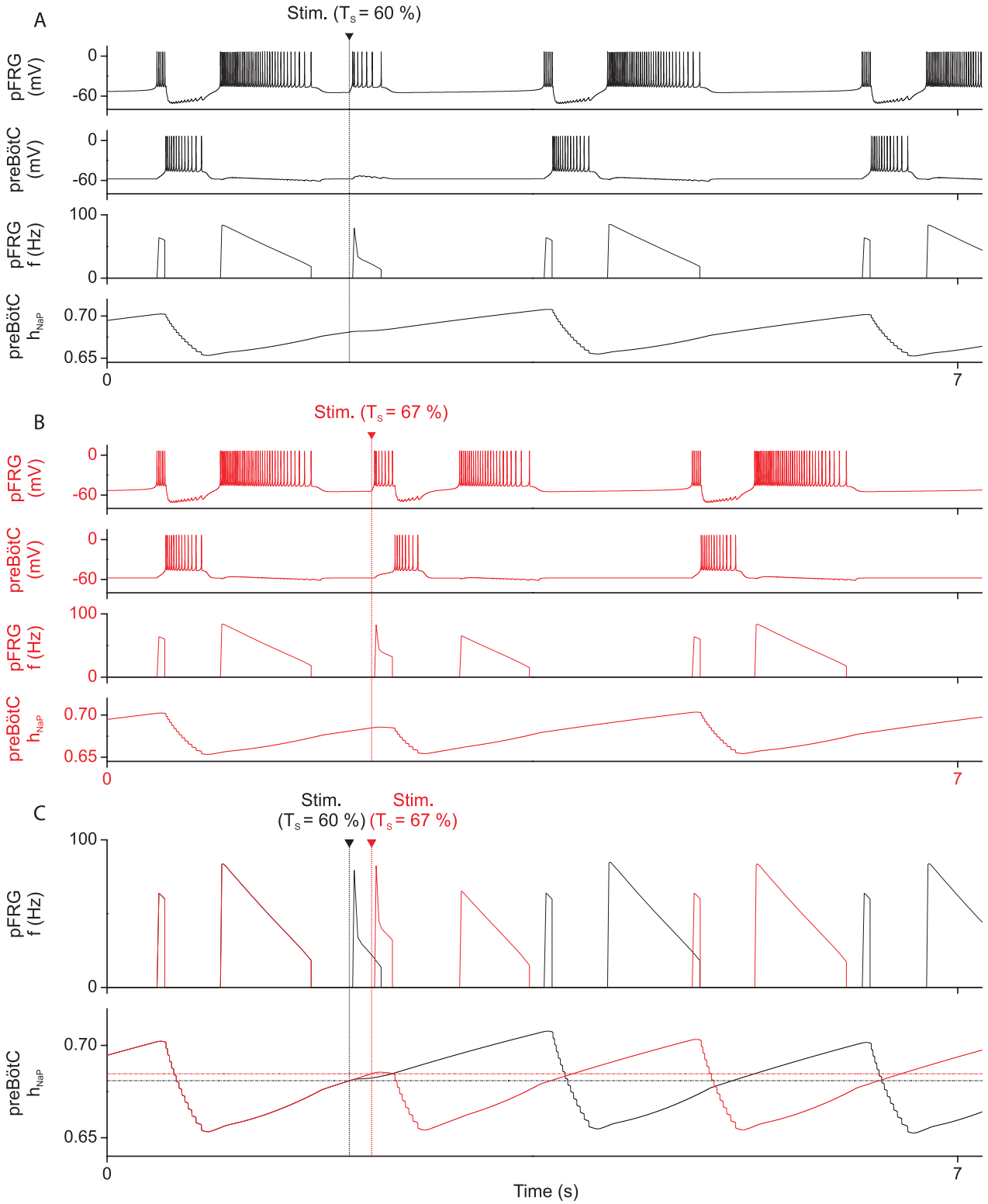

Fig. S1. Simulation of pFRG stimulation. (*A*) Stimulation at 60% of the preBötC cycle evoked a low-frequency pFRG burst that prolonged expiration. (*B*) Stimulation at 67% evoked a premature preBötC burst and reset the respiratory rhythm. (*C*) Comparison of pFRG burst frequency and of preBötC Na_P inactivation variable *h* for stimulations applied at 60% and 67% of the preBötC cycle. During silent periods, the inactivation gating variable *h* of the burst generating persistent sodium channels relaxes to its resting state with the time constant $\bar{\tau}_h$, which results in a gradual increase in cell excitability. Hence, stimulations applied later during expiration lower the activation threshold of the preBötC and evoke pFRG bursts with higher frequencies which increases the excitatory drive to the preBötC and causes a premature preBötC burst.

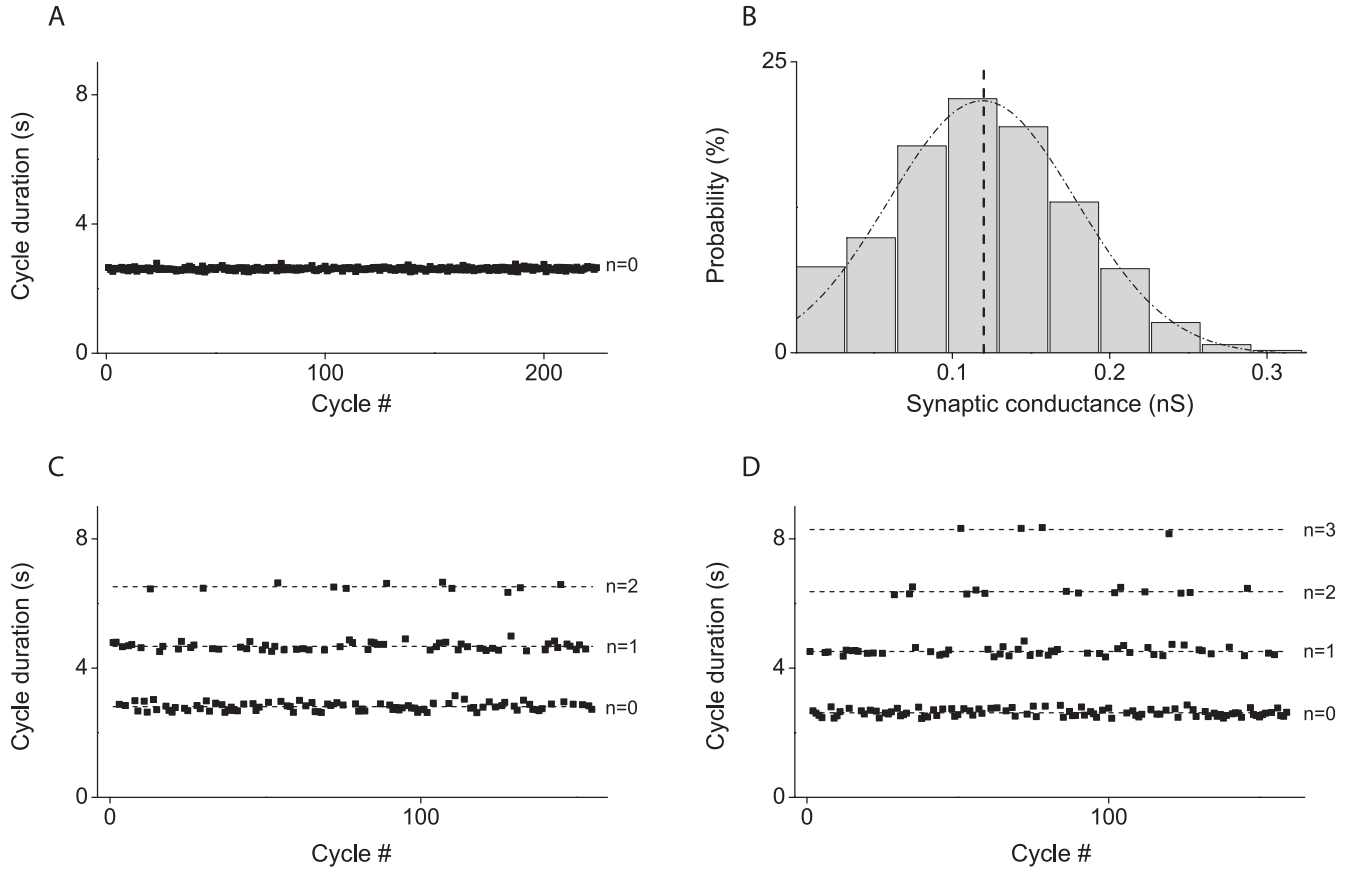

Fig. S2. Simulation of opioid-induced quantal breathing. (*A*) Under default conditions (no preBötC hyperpolarization, no excitatory drive reduction) no respiratory cycles are skipped ($n = 0$), and all cycle durations are distributed around the mean default cycle time ($\bar{T}_C = 2.6$ s). (*B*) Example for the Gaussian-distributed excitatory drive of the stochastic preBötC synapse with mean $\mu_E = 0.12$ nS and variance $\sigma_E = 0.06$ nS. Negative conductances were set to 0. (*C*) Example for preBötC cycle duration distribution when only presynaptic suppression was modeled. ($\mu_E = 0.066$ nS, $\sigma_E = 0.033$ nS; 55% of control). (*D*) Example for preBötC cycle duration distribution when only postsynaptic suppression (hyperpolarization) was modeled (≈3.6 mV; $E_L = -63$ mV).

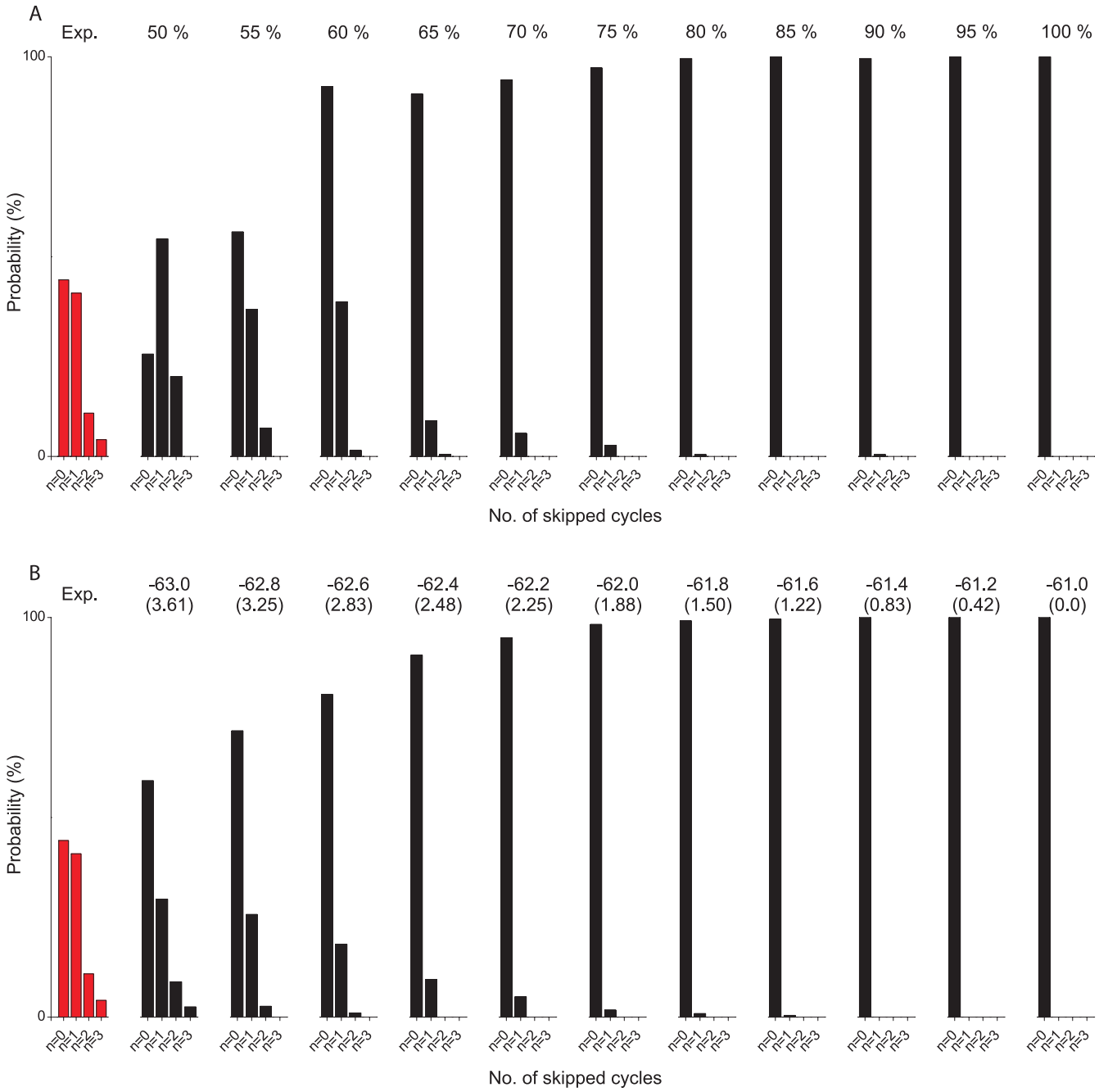

Fig. S3. Simulation of opioid-induced quantal breathing. (*A*) Distribution of skipped cycle probabilities when only presynaptic preBötC suppression was modeled. The mean and variance of the excitatory stochastic preBötC synapse (μ_E and σ_E, respectively) were hereby gradually decreased from 100% to 50% in steps of 5%. (*B*) Distribution of skipped cycle probabilities when only postsynaptic preBötC suppression was included. preBötC hyperpolarization was modeled by gradual reduction of the leak reversal potential E_L (−61 mV to −63 mV in steps of −0.2 mV). The resulting hyperpolarization (in millivolts) is shown in parentheses.

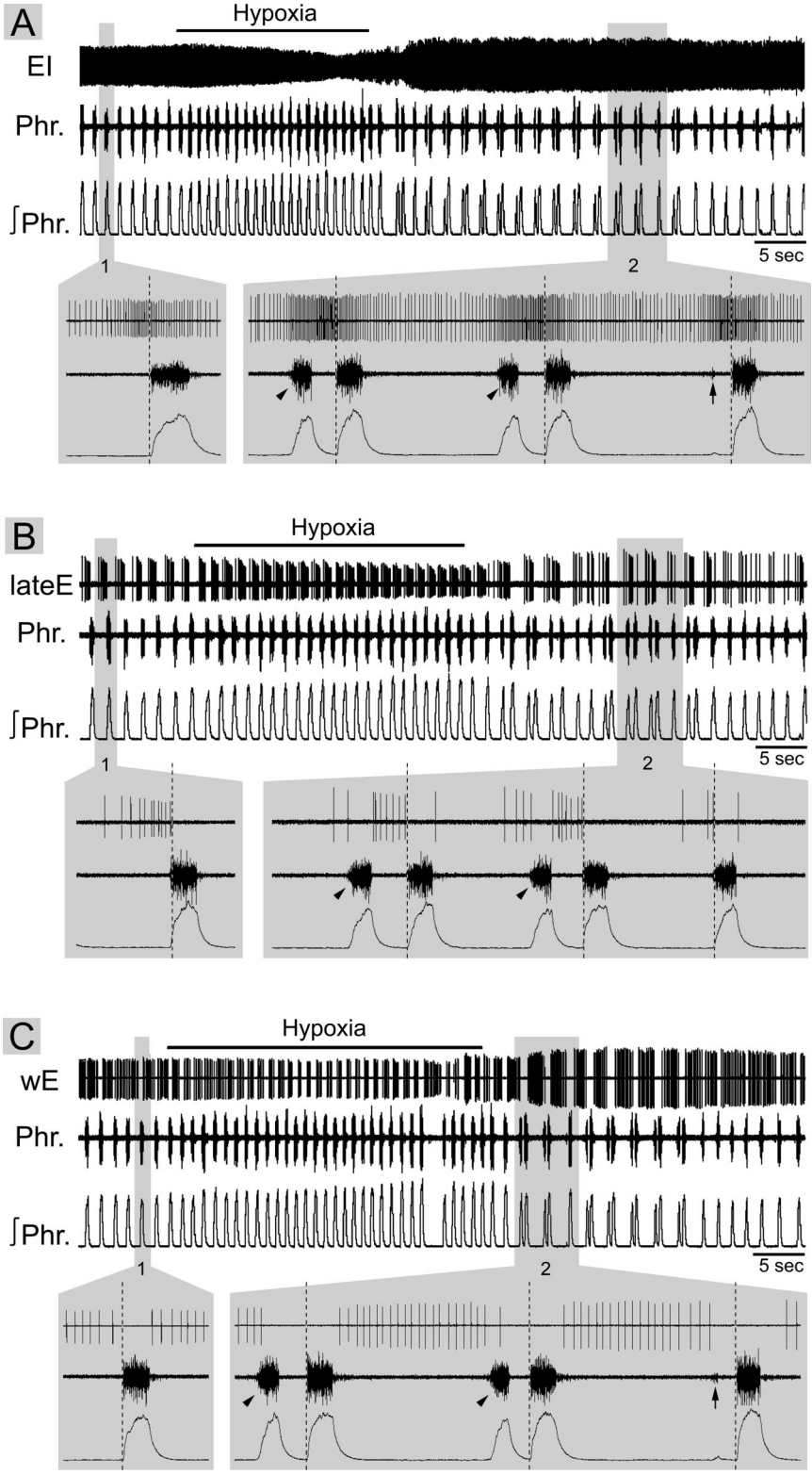

Fig. S4. Double bursts in phrenic discharge recorded during recovery from hypoxia. Normal phrenic bursts and posthypoxia double bursts are shown in relation to the discharges of 3 respiratory neurons recorded from the dorsolateral pons pneumotaxic center. (*A*) Expiratory–inspiratory phase-spanning unit. (*B*) Late expiratory unit. (*C*) Whole-phase expiratory unit. *Insets* show enlarged views of the recordings in control (*Inset* 1) and posthypoxia phase (*Inset* 2). Arrowheads indicate premature inspiratory burst. Arrows indicate maldeveloped premature bursts.

Table S1. Model parameters of the ionic currents I_{NaF}, I_{KDr}, I_{NaP}, and I_{Leak}

	Na_F				K_{Dr}					Na_P							Leak	
	$\bar{g}_{NaF}$ nS	θ_m mV	σ_m mV	E_{Na} mV	$\bar{g}_{KDr}$ nS	θ_n mV	σ_n mV	$\bar{\tau}_n$ ms	E_K mV	$\bar{g}_{NaP}$ nS	θ_k mV	σ_k mV	θ_h mV	σ_h mV	$\bar{\tau}_h$ ms	E_{Na} mV	g nS	E mV
pFRG	28	−34	−5	50	11.2	−29	−4	10	−77	3.75	−40	−6	−48	6	7,000	50	2.8	−59
preBötC	28	−34	−5	50	11.2	−29	−4	10	−77	2.5	−40	−6	−48	6	10,000	50	2.8	−61